


ORIGINAL RESEARCH PAPER

Constrained optimised flexible power control for grid-connected converters under unbalanced faults

Nabila Ahmed Rufa'I  | Li Zhang | Benjamin ChongSchool of Electronic and Electrical Engineering,
University of Leeds, Leeds, UK**Correspondence**Nabila Ahmed Rufa'I, School of Electronic and
Electrical Engineering, University of Leeds, LS2 9JT,
Leeds, UK.
Email: e112nari@leeds.ac.uk; nabilarufai@gmail.com**Abstract**

This paper presents a constrained multi-objective optimisation scheme for a grid-connected voltage source converter operating under unbalanced voltage conditions in a three-phase three-wire system. The scheme is aimed at evaluating the converter reference currents required to supply all the power generated by the connected source to the grid, whilst simultaneously suppressing oscillations of both real and reactive powers. The trade-off between these two conflicting requirements is achieved by setting a single cost function with variable weightings. Two constraints are set to restrict the converter instantaneous phase current and maintain low DC-bus voltage percentage ripple. A genetic algorithm is applied to search for the optimal solution. Simulation results are presented and confirm the effectiveness of the proposed method.

1 | INTRODUCTION

The rapid penetration of renewable energy sourced generators into the utility network has resulted in many grid-connected voltage source converters (VSCs) being connected to the distribution lines and load centres. These converters and their control schemes are generally designed to operate under normal grid voltage conditions. However, a power grid is a dynamic system whose operation is affected by many factors, one of the most common being voltage unbalance, accounting for over 90% of all faults [1, 2]. A major cause of voltage unbalance may not be fault related, but the uneven distribution of single-phase loads. These can be continuously changing across three-phase power systems. Under unbalanced conditions, the grid-connected VSCs would cause unbalanced and distorted currents to be injected into the grid, which may result in high losses and overcurrent damage. Disconnection of grid-tie converters under such conditions may not be an option, because with an increasing proportion of power being renewably generated, they may have become indispensable to the power network. Grid codes now require these systems, particularly with wind powered generators, to ride through voltage dips without interruption [3, 4].

Active R&D efforts have been directed to ensuring robust operation of grid-tie converters under unbalanced conditions

[5]. The two main objectives are to mitigate unbalanced voltages at the point of common connection (PCC) and to eliminate active and/or reactive power oscillations. While the former relies on the injection of reactive currents using devices such as static voltage controllers [6], the latter relies on grid converter control and poses more challenges. This is due to the negative sequence component in unbalanced voltages at the PCC [7] (three-phase three wire case) inevitably inducing negative-sequence current in the converter. The products of current and voltage of different sequences result in oscillatory real and reactive powers at mainly twice the line frequency. These may be exacerbated by DC-link voltage fluctuations due to the instantaneous input and output power mismatch. Proper control of unbalanced current injected to the grid can alleviate the power oscillation. This relies on two crucial aspects: estimating the reference current to be injected by setting specific control objectives, and having current control laws to track effectively the calculated reference value. The control objectives can be many and some common cases are discussed in detail in [4, 7-9], which include: controlling the average real or reactive power, cancellation of active power oscillations while ensuring delivery of the maximum generated real power and grid required reactive power, or the cancellation of reactive power oscillations, etc. These result in different overall performance of the inverters

This is an open access article under the terms of the [Creative Commons Attribution](https://creativecommons.org/licenses/by/4.0/) License, which permits use, distribution and reproduction in any medium, provided the original work is properly cited.

© 2021 The Authors. *The Journal of Engineering* published by John Wiley & Sons Ltd on behalf of The Institution of Engineering and Technology

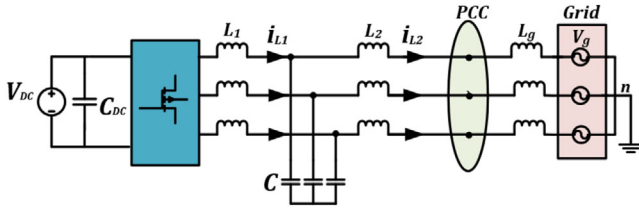


FIGURE 1 Three-phase grid connected converter with LCL filter

and their interactions with the grid under unbalanced conditions may not be desirable for certain application conditions. An adequate criterion should ensure accurate control of the dominant variables, for example, the source-generated power, while maintaining the other variables within the grid tolerable ranges. It is also important that the inverter supplied current must be constrained to prevent overcurrent tripping [4]. It is possible to deduce new alternative control strategies based on the existing ones [9, 10] by imposing certain constraints. The resultant reference currents may be more suitable to be injected into the grid by the grid-connected inverters.

This paper, therefore, proposes a new constrained optimised flexible power control (COFPC) scheme based on the principle of the constrained multi-objective optimisation problem (MOOP). The objective is to ensure that the grid connected inverter supplies the power from its renewable source to the grid, maintaining unity power factor whilst simultaneously dealing with the conflicting requirements of suppressing real and reactive power oscillations. Under such a control law, the inverter should be able to ride through unbalanced grid faults. A single cost function with weightings and constraints will be defined. The constraints set will limit the DC-bus voltage ripple and restrict the inverter instantaneous phase current magnitude to be below its rated level. A genetic algorithm (GA) will be used to search for the optimised solution for the cost function. The performance of the proposed method is validated through simulation studies and compared with two other major unbalanced current control schemes for the grid-connected inverters.

The remaining sections of the paper are organised as follows: Section 2 presents the derivation of key equations for the active and reactive powers supplied to the grid and their oscillations. Section 3 derives the reference currents for the COFPC scheme based on a grid-connected VSC with an LCL filter. Section 4 outlines the multi-objective optimisation (MOO) criteria for minimisation of active and reactive power ripples subject to the specified constraints. Section 5 describes the process of optimising the control scheme using GA. Section 6 describes the control system and Section 7 presents the simulation results.

2 | ACTIVE AND REACTIVE POWERS UNDER UNBALANCED GRID CONDITIONS

A three-phase grid-tie converter is connected to the power lines via an LCL filter as shown in Figure 1. L_1 and L_2 are filter inductances at the inverter terminals, and C is the filter capacitance.

L_g represents the grid-line inductance. The DC voltage source, V_{DC} is maintained by a renewable energy source such as a PV or a wind power generator.

To analyse this system, the following assumptions are made:

- The generator connected on the DC bus has a slow dynamic response speed and the weather conditions are not changed; hence, power output to the grid are assumed constant.
- The neutral points of the distribution network and the converter are not connected; hence it has three-phase three-wire connection. Hence, there is no zero sequence current flow under unbalanced conditions.

When grid voltages at the PCC and currents flowing to the grid are unbalanced, they can be decomposed into the positive and negative symmetrical components by applying Fortescue theorem, and when only fundamental elements are considered, they are:

$$v_g = V_p \sin\left(\omega t + \varphi_{vp} - k\frac{2\pi}{3}\right) + V_n \sin\left(-\omega t + \varphi_{vn} - k\frac{2\pi}{3}\right) \quad (1)$$

and

$$i_g = I_p \sin\left(\omega t + \varphi_{ip} - k\frac{2\pi}{3}\right) + I_n \sin\left(-\omega t + \varphi_{in} - k\frac{2\pi}{3}\right), \quad (2)$$

where V_p and V_n are the positive and negative sequence voltages with phase angles φ_{vp} and φ_{vn} , I_p and I_n are the positive and negative sequence currents with phase angles φ_{ip} and φ_{in} , $m = a, b, c$ and $k = 0, 1, -1$ for phases a, b, c respectively.

Projecting both three-phase voltage and current on the positive and negative synchronous reference frames (SRF) [11] rotating synchronously at $+\omega$ and $-\omega$ respectively leads to v_{dq}^+ and v_{dq}^- which are expressed as:

$$v_{dq}^+ = \begin{bmatrix} v_d^+ \\ v_q^+ \end{bmatrix} + \begin{bmatrix} \tilde{v}_d^+ \\ \tilde{v}_q^+ \end{bmatrix} = V_p^+ \begin{bmatrix} \cos \varphi_{vp} \\ \sin \varphi_{vp} \end{bmatrix} + V_p^- \begin{bmatrix} \cos 2\omega t & \sin 2\omega t \\ -\sin 2\omega t & \cos 2\omega t \end{bmatrix} \begin{bmatrix} \cos \varphi_{vn} \\ \sin \varphi_{vn} \end{bmatrix} \quad (3)$$

and

$$v_{dq}^- = \begin{bmatrix} v_d^- \\ v_q^- \end{bmatrix} + \begin{bmatrix} \tilde{v}_d^- \\ \tilde{v}_q^- \end{bmatrix} = V_n^- \begin{bmatrix} \cos \varphi_{vn} \\ \sin \varphi_{vn} \end{bmatrix} + V_n^+ \begin{bmatrix} \cos 2\omega t & -\sin 2\omega t \\ \sin 2\omega t & \cos 2\omega t \end{bmatrix} \begin{bmatrix} \cos \varphi_{vp} \\ \sin \varphi_{vp} \end{bmatrix}. \quad (4)$$

Similarly, i_d^{\pm}, i_q^{\pm} formulae can be derived. Note the derivations of the above must be based on an accurate phase locking

loop to identify the phase angles of the grid positive and negative sequence voltages, φ_{vp} and φ_{vm} .

Subsequently, according to the instantaneous power theory [7, 12], the instantaneous real and reactive powers generated by a three-phase converter operating under unbalanced grid conditions can be calculated as:

$$p = (v_d^+ + v_q^+ + v_d^- + v_q^-) \cdot (i_d^+ + i_q^+ + i_d^- + i_q^-) \quad (5)$$

and

$$q = (v_d^+ + v_q^+ + v_d^- + v_q^-) \times (i_d^+ + i_q^+ + i_d^- + i_q^-). \quad (6)$$

The resultant formulae from the above are:

$$p = P + P_c \cos(2\omega t) + P_s \sin(2\omega t) \quad (7)$$

and

$$q = Q + Q_c \cos(2\omega t) + Q_s \sin(2\omega t), \quad (8)$$

where P and Q are the average values of the instantaneous active and reactive powers, P_c , P_s , Q_c and Q_s are the amplitudes of the oscillating terms associated with the two powers respectively. These amplitudes are evaluated as:

$$P = \frac{3}{2} (v_d^+ i_d^+ + v_q^+ i_q^+ + v_d^- i_d^- + v_q^- i_q^-) \quad (9)$$

$$P_c = \frac{3}{2} (v_d^- i_d^+ + v_q^- i_q^+ + v_d^+ i_d^- + v_q^+ i_q^-) \quad (10)$$

$$P_s = \frac{3}{2} (v_q^- i_d^+ - v_d^- i_q^+ - v_q^+ i_d^- + v_d^+ i_q^-) \quad (11)$$

$$Q = \frac{3}{2} (v_q^+ i_d^+ - v_d^+ i_q^+ + v_q^- i_d^- - v_d^- i_q^-) \quad (12)$$

$$Q_c = \frac{3}{2} (v_q^- i_d^+ - v_d^- i_q^+ + v_q^+ i_d^- - v_d^+ i_q^-) \quad (13)$$

and

$$Q_s = \frac{3}{2} (-v_d^- i_d^+ - v_q^- i_q^+ + v_d^+ i_d^- + v_q^+ i_q^-). \quad (14)$$

The common objective for controlling a grid-tie converter is to ensure that the real power, P , generated by the power source is delivered to the grid. Also depending on the grid requirement, a given reactive power, Q , may be injected to the grid to improve the power factor, while all oscillatory real and reactive power elements should be suppressed. Such objectives rely on proper evaluations of converter reference current. From Equations (9) to (14), there are only four current elements, i_d^\pm and i_q^\pm available for controlling six power terms. This makes it difficult

to suppress both P and Q fluctuation components concurrently while ensuring ripple free real power exchange between the DC-bus and AC grid. The choice of the power parameters to be controlled is, therefore, dependent on the desired criteria. For example, to maintain DC voltage constant and free from oscillations, the active power oscillations must be controlled ideally to zero, consequently the reactive power ripple remains uncontrolled. On the other hand, if the desire is to suppress reactive power ripples, active power ripples may be left intact. Thus, there are many solutions depending on the choice of applications.

3 | CONSTRAINED OPTIMISED FLEXIBLE POWER CONTROL (COFPC) SCHEME

This proposed scheme adopts the strategy given by [7, 13], namely, the flexible power control (FPC) scheme and re-defines it as a constrained MOOP for reference current estimation. The flexibility lies in setting the control objectives. For example, the objectives can be supplying a constant active power, P^* to the grid based on the source-generated power and a constant reactive power, Q^* according to the grid required power factor. Also, suppressing both active power oscillations is required. Then, according to Equations (9) to (12), the reference d - q current elements can be derived as:

$$\begin{bmatrix} i_d^{+*} \\ i_q^{+*} \\ i_d^{-*} \\ i_q^{-*} \end{bmatrix} = \begin{bmatrix} v_d^+ & v_q^+ & v_d^- & v_q^- \\ v_q^+ & -v_d^- & v_q^- & -v_d^- \\ v_d^- & -v_q^- & v_d^+ & v_q^+ \\ v_q^- & -v_d^- & -v_q^+ & v_d^+ \end{bmatrix}^{-1} \begin{bmatrix} P^* \\ Q^* \\ 0 \\ 0 \end{bmatrix}. \quad (15)$$

Simplifying Equation (15) and assuming unity power factor, the reference currents can be computed as:

$$\begin{bmatrix} i_d^{+*} \\ i_q^{+*} \\ i_d^{-*} \\ i_q^{-*} \end{bmatrix} = \frac{P^*}{1.5 [\|v_d^+\|^2 + \|v_q^+\|^2 - [\|v_d^-\|^2 + \|v_q^-\|^2]]} \begin{bmatrix} v_d^+ \\ v_q^+ \\ -v_d^- \\ -v_q^- \end{bmatrix}. \quad (16)$$

On the other hand, if the control requirements are changed to maintaining P and Q by only injecting positive sequence components into the grid, the reference current d - q components are determined by considering only Equations (9) and (12), with no negative sequence current components considered. Thus, by setting the reference real and reactive powers, P^* and Q^* in these two equations, the two positive sequence reference current elements are given as:

$$\begin{bmatrix} i_d^{+*} \\ i_q^{+*} \end{bmatrix} = -\frac{1}{1.5 [\|v_d^+\|^2 + \|v_q^+\|^2]} \begin{bmatrix} -v_d^+ & -v_q^+ \\ -v_q^+ & v_d^+ \end{bmatrix} \begin{bmatrix} P^* \\ Q^* \end{bmatrix}. \quad (17)$$

For unity power factor operation, Q^* is zero, so the reference currents are reduced to:

$$\begin{bmatrix} i_d^{+*} \\ i_q^{+*} \end{bmatrix} = \frac{P^*}{1.5 \left[\|v_d^+\|^2 + \|v_q^+\|^2 \right]} \begin{bmatrix} v_d^+ \\ v_q^+ \end{bmatrix}. \quad (18)$$

It is clear that this method can achieve real and reactive power control at the expense of leaving all oscillatory terms, P_c , P_s , Q_c and Q_s given in Equations (10), (11), (13) and (14) respectively, unconstrained. On the other hand, the control aim can instead be set to cancel all reactive power oscillations whilst keeping desired P^* and Q^* . This renders the active powers oscillations, P_C and P_S uncontrolled. The corresponding four current references derived from Equations (9), (12) to (14) are expressed as:

$$\begin{bmatrix} i_d^{+*} \\ i_q^{+*} \\ i_d^{-*} \\ i_q^{-*} \end{bmatrix} = \begin{bmatrix} v_d^+ & v_q^+ & v_d^- & v_q^- \\ v_q^+ & -v_d^+ & v_q^- & -v_d^- \\ v_q^- & -v_d^- & v_q^+ & -v_d^+ \\ -v_d^- & -v_q^- & v_d^+ & v_q^+ \end{bmatrix}^{-1} \begin{bmatrix} P^* \\ Q^* \\ 0 \\ 0 \end{bmatrix}. \quad (19)$$

Upon simplification of Equation (19) with unity power factor, these reference current elements are given as:

$$\begin{bmatrix} i_d^{+*} \\ i_q^{+*} \\ i_d^{-*} \\ i_q^{-*} \end{bmatrix} = \frac{P^*}{1.5 \left[\|v_d^+\|^2 + \|v_q^+\|^2 + \left[\|v_d^-\|^2 + \|v_q^-\|^2 \right] \right]} \begin{bmatrix} v_d^+ \\ v_q^+ \\ v_d^- \\ v_q^- \end{bmatrix}. \quad (20)$$

Similar to Equation (16), this also leads to injecting non-sinusoidal currents to control P and Q , while suppressing only the reactive power harmonics.

Based on the above derived equations, it is possible to introduce a variable κ , in the range $-1 \leq \kappa \leq 1$ into Equations (16), (18) and (20) to accommodate flexibly different control objectives. Consequently, the reference currents can be expressed as:

$$\begin{bmatrix} i_d^{+*} \\ i_q^{+*} \\ i_d^{-*} \\ i_q^{-*} \end{bmatrix} = \frac{P^*}{1.5 \left[\|v_d^+\|^2 + \|v_q^+\|^2 + \kappa \left[\|v_d^-\|^2 + \|v_q^-\|^2 \right] \right]} \begin{bmatrix} v_d^+ \\ v_q^+ \\ \kappa v_d^- \\ \kappa v_q^- \end{bmatrix}. \quad (21)$$

When κ is -1 , the active power oscillations are eliminated, as in the case of constant active power control (CAPC) of Equation (16) [7]. With κ set to 0, only positive sequence current elements are injected into the grid since all negative sequence components are eliminated, as in the balanced positive sequence control (BPSC) of Equation (18) [7, 8]. Finally, setting κ to 1

removes reactive power oscillations, as in the constant reactive power control described by Equation (20) [7].

Using the approach stated above, the total amount of active and reactive power ripples, $P_{rip} = P_C + P_S$ and $Q_{rip} = Q_C + Q_S$ can be computed by substituting the currents expressed in Equation (21) into the oscillatory power expressions in Equations (10), (11), (13) and (14) as:

$$P_{rip} = \frac{P^* (1 + \kappa) (v_d^+ v_d^- + v_q^+ v_q^- + v_d^+ v_q^- - v_d^- v_q^+)}{\|v_d^+\|^2 + \|v_q^+\|^2 + \kappa \left[\|v_d^-\|^2 + \|v_q^-\|^2 \right]} \quad (22)$$

and

$$Q_{rip} = \frac{P^* (1 - \kappa) (v_d^+ v_q^- - v_d^- v_q^+ - v_d^+ v_d^- - v_q^+ v_q^-)}{\|v_d^+\|^2 + \|v_q^+\|^2 + \kappa \left[\|v_d^-\|^2 + \|v_q^-\|^2 \right]} \quad (23)$$

Within the feasible range for κ ($-1 \leq \kappa \leq 1$), Equation (22) and (23) enable evaluations of P_{rip} and Q_{rip} as:

$$P_{rip} = \begin{cases} 0 & \kappa = -1 \\ \frac{P^* (v_d^+ v_d^- + v_q^+ v_q^- + v_d^+ v_q^- - v_d^- v_q^+)}{\|v_d^+\|^2 + \|v_q^+\|^2} & \kappa = 0 \\ \frac{2P^* (v_d^+ v_d^- + v_q^+ v_q^- + v_d^+ v_q^- - v_d^- v_q^+)}{\|v_d^+\|^2 + \|v_q^+\|^2 + \left[\|v_d^-\|^2 + \|v_q^-\|^2 \right]} & \kappa = +1 \end{cases} \quad (24)$$

and

$$Q_{rip} = \begin{cases} \frac{2P^* (v_d^+ v_q^- - v_d^- v_q^+ - v_d^+ v_d^- - v_q^+ v_q^-)}{\|v_d^+\|^2 + \|v_q^+\|^2 - \left[\|v_d^-\|^2 + \|v_q^-\|^2 \right]} & \kappa = -1 \\ \frac{P^* (v_d^+ v_q^- - v_d^- v_q^+ - v_d^+ v_d^- - v_q^+ v_q^-)}{\|v_d^+\|^2 + \|v_q^+\|^2} & \kappa = 0 \\ 0 & \kappa = +1 \end{cases} \quad (25)$$

It is worth noting that the choice of these control objectives may lead to the converter injecting unbalanced three phase currents to the grid. The instantaneous phase current values need to be checked and clamped if necessary, to prevent over-current tripping of the converter, so current constraint must be applied while searching for the optimal κ value. There are also other constraints which are important for grid-connected inverters under unbalanced voltage operations. These include the percentage limit of the DC-bus voltage ripple relative to the required average voltage level and the maximum value of the reference current.

Thus, the optimal κ is the value which not only must satisfy two conflicting objectives; i.e., minimising both P_{rip} and Q_{rip} , while simultaneously giving the required active and reactive powers, but also should meet the required constraints. This gives rise to a new power control technique; namely, the COFPC.

4 | MOOP-BASED SOLUTION FOR COFPC

MOOP concerns an area of multiple decision making, where a problem can involve multiple objective functions that need to be optimised simultaneously. One approach involves converting the MOOP into a single cost function by using a weighted sum of multiple objective functions [14]. A solution to this sum leads to an optimal choice for the original problem, forming the Pareto front [15]. The search for the optimal solution can be further narrowed down through the introduction of constraints.

4.1 | Defining cost function

Since it may not be possible to find one set of reference current elements which are optimal to both objective functions specified in Equations (22) and (23), a single cost function can be defined as [14, 15]:

$$\min F(k) = [f_1(k), f_2(k)], \quad (26)$$

where $f_1(k)$ is the active power ripple defined by Equation (22) and $f_2(k)$ is the reactive power ripple defined by Equation (23). A preference-based method is employed to convert this MOOP into a single objective optimisation problem using preference factors w_1 and w_2 assigned to each objective [14, 16, 17]. Thus:

$$F(k) = w_1 f_1(k) + w_2 f_2(k), \quad (27)$$

with w_1, w_2 cumulatively summing up to 1. Each set of w_1, w_2 results in an optimal k value. This k value leads to a set of reference current values optimal to the corresponding unbalanced voltage values and power requirements. This represents a Pareto solution. Note that k takes any value between -1 and 1 .

4.2 | Objective function weightings

This is to choose w_1 and w_2 in Equation (27) which may be the same or different. Considering the empirical knowledge regarding the optimisation problem, differential weights are preferable [17]. The weighted sum in Equation (27) uses a priori articulation of preferences, with the weights assigned directly based on their relative importance, as per the rating method [18]. The main criticism regarding this approach is its inherent difficulty in accurately determining the Pareto front [19]. It does, however, prove a useful tool for a single optimisation problem such as Equation (27).

In terms of relative importance, the active power ripple function, $f_1(k)$ is prioritised over the reactive power ripple function, $f_2(k)$, therefore w_1 should be set greater than w_2 . However, the constraint based on the DC link fluctuations, ΔV will impose a restriction on the decision variable, k which favours the minimisation of $f_1(k)$ in the objective function. Figure 2 shows the decision variable, k obtained for different weight ratios under a PCC voltage unbalance factor of 7%. It can be

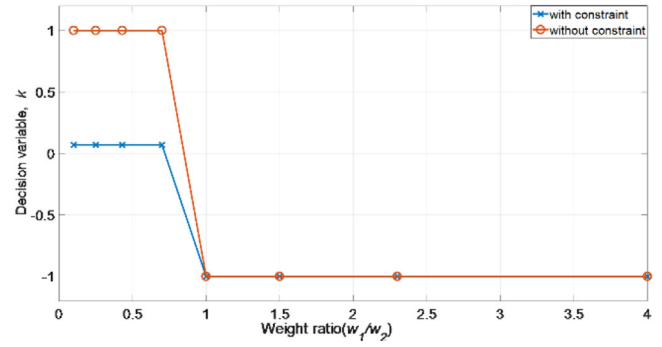


FIGURE 2 Assigned weight variation with decision variable

observed that when w_1/w_2 is less than unity, the decision variable, k has a value of 0.07 as imposed by the optimisation constraints. However, when w_1/w_2 is greater than 1, the minimisation algorithm favours complete active ripple attenuation, with $k = -1$. Hence, it is imperative that w_2 be set higher than w_1 to ensure that the contribution of $f_2(k)$ is inclusive in the minimisation problem.

4.3 | Setting optimisation constraints

Two constraints are defined to ensure that the optimal value for k leads to reference current values satisfactory to the required objectives. These are as follows:

4.3.1 | DC link voltage fluctuation

The level of low frequency DC link voltage fluctuation (ΔV) directly relates to the maximum value of the active power ripple ($P_{rip(max)}$) through the following [20]:

$$P_{rip(max)} = \omega C V_{DC} \Delta V, \quad (28)$$

where C is the capacitance of the DC link capacitor, V_{DC} is the mean DC link voltage and ω is the grid frequency. The choice of the C value has a direct effect on the DC voltage fluctuation: a high value reduces the magnitude of the ripple, but results in increased size and cost. For a given value of C , the active power ripple can be constrained based on:

$$P_{rip} \leq P_{rip(max)}. \quad (29)$$

The maximum voltage ripple is generally limited to 1% to 2% of the DC link voltage [21]. On the basis of this constraint, substituting Equations (22) and (28) into (29) we have:

$$k \leq \frac{\omega C V_{DC} \Delta V \left[\|v_d^+\|^2 + \|v_q^+\|^2 \right] - P(v_d^+ v_d^- + v_q^+ v_q^- + v_d^+ v_q^- - v_d^- v_q^+)}{P(v_d^+ v_d^- + v_q^+ v_q^- + v_d^+ v_q^- - v_d^- v_q^+) - \omega C V_{DC} \Delta V \left[\|v_d^-\|^2 + \|v_q^-\|^2 \right]}. \quad (30)$$

4.3.2 | Maximum converter phase current

This constraint is necessary to protect the converter from over-current tripping. Under unbalanced voltage, the per phase current through the converter can be expressed in the stationary reference frame as:

$$I = \sqrt{I^{+2} + I^{-2} + 2I^+I^- \cos \alpha}, \quad (31)$$

where I^+ and I^- are the magnitudes of the positive and negative sequence current components. After manipulations (see the Appendix) the per phase maximum current is given as:

$$I_{m(\max)} = \frac{P \sqrt{\|v_d^+\|^2 + \|v_q^+\|^2 + \kappa^2 [\|v_d^-\|^2 + \|v_q^-\|^2]} + 2\kappa \sqrt{[\|v_d^+\|^2 + \|v_q^+\|^2] [\|v_d^-\|^2 + \|v_q^-\|^2]}}{1.5 [\|v_d^+\|^2 + \|v_q^+\|^2 + \kappa [\|v_d^-\|^2 + \|v_q^-\|^2]]} \quad (32)$$

where m represents phases a, b, c .

To avoid device tripping due to overcurrent, the maximum current per phase should be less than the converter rated current value, so

$$I_{m(\max)} \leq I_{rated}. \quad (33)$$

I_{rated} is normally determined by the maximum power the source can generate under balanced conditions as:

$$I_{rated} = \frac{P}{1.5V^+}, \quad (34)$$

where V^+ is the magnitude of the positive sequence grid voltage expressed as:

$$V^+ = \sqrt{\|v_d^+\|^2 + \|v_q^+\|^2} \quad (35)$$

When the voltage unbalanced factor (VUF), that is, the ratio of negative sequence to positive sequence voltages, increases, v_d^- and v_q^- rise naturally, the maximum converter current defined in Equation (32) increases. Depending on the degree of unbalance, $I_{m(\max)}$ may exceed I_{rated} . To prevent this, the active power reference, P^* should be reduced to ensure the corresponding I_{rated} is lower than the normal rated value under balanced voltages. Thus, the new reference active power is determined from Equation (34) as:

$$P^* = \frac{3}{2} I_{rated} V^+. \quad (36)$$

It should be noted that the large current fluctuations that are above the current limit of the converter cannot be ade-

quately controlled by the proposed control system due to the current limit constraint that protects the inverter switches from damages. Due to this reason, the proposed control system is limited to operate only within the limit of the inverter maximum current.

5 | CONSTRAINED OPTIMAL SOLUTION BY GENETIC ALGORITHM

The search for the solution involves three procedures; applying GA searching methods [15, 22] to find the optimal κ value, verifying the searched value to satisfy the constraints and evalu-

ating the reference currents for applying into the control loop. GAs, like many other evolutionary algorithms, have the distinct advantage of searching for solutions by operating in parallel. This makes it easier to discover the global optimum solution, unlike traditional methods which search from a singular point [23]. Additionally, they are capable of providing effective solutions to nonconvex problems [24].

5.1 | GA searching for optimal κ

In the first step, before embarking on the optimal κ searching using GA method, the range of κ for the specified voltage ripple constraint, ΔV , needs to be evaluated using Equation (30).

The GA is applied to search for the optimal κ value which minimises the cost function defined by Equation (27). GA technique is based on Darwin's theory of natural selection which derives the optimal solution through modification of a population by using certain operators at each step in the evolution process. The main operators are: selection, crossover and mutation.

The GA process of minimising Equation (27) can be summarised as follows [25]:

1. Generate a random population of κ values with lower and upper bounds of -1 and $+1$.
2. For each κ in the population, evaluate its corresponding fitness function based on Equation (27) and determine the best individuals to form the next population.
3. The next generation is produced by the following steps:
 - I. Select two chromosomes from the selected population to form an offspring by crossover,
 - II. Apply random changes to individual chromosomes to form offspring by mutation,

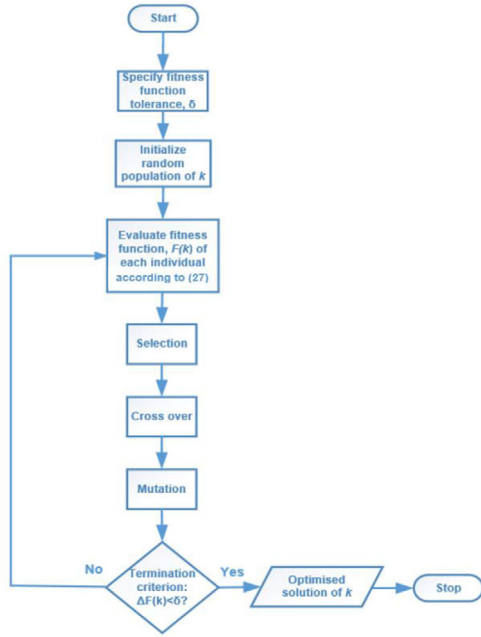


FIGURE 3 Flow chart for genetic algorithm (GA)

- III. Select the new generation based on the fitness function.
4. Replace the initial population with the new generation.
5. Terminate if stopping criteria (convergence) is met, otherwise return to Step 2.

The GA process terminates when a convergence criterion is met. In this case, it is set as the fitness function tolerance factor, δ , which evaluates the average change in the value of the fitness function, $\Delta F(k)$, over a number of generations known as stall generations. If $\Delta F(k)$ is less than or equal to δ , the problem has converged to an optimal solution. On the other hand, if $\Delta F(k)$ is greater than δ , the process is renewed with a new set of chromosomes. The genetic algorithm process of finding the optimal value of k can be seen in Figure 3

5.2 | Verification for constraints and evaluation of reference current

Since the constraint for DC-bus voltage ripple is already embedded in Equation (27), the only other constraint for verification of the optimised k is the maximum current. If the resultant $I_{m(max)}$ is less than the rated value, the reference currents for the inverter current control can be computed directly using Equation (21). Otherwise, a new reduced reference active power, P^* needs to be set from Equation (36). Subsequently, a new set of inverters rated current is determined from Equation (21). Based on the above descriptions of reference current evaluation principle, a flowchart describing the whole procedure including the application of constraints is given in Figure 4.

It is worth noting that the determination of k using MOOP for COFPC scheme as presented above is performed off-line, according to the measured PCC voltage. For different three-

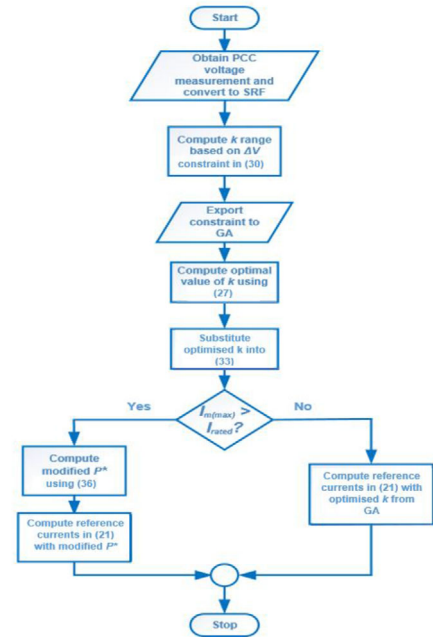


FIGURE 4 Flow chart for constraint and reference current generation

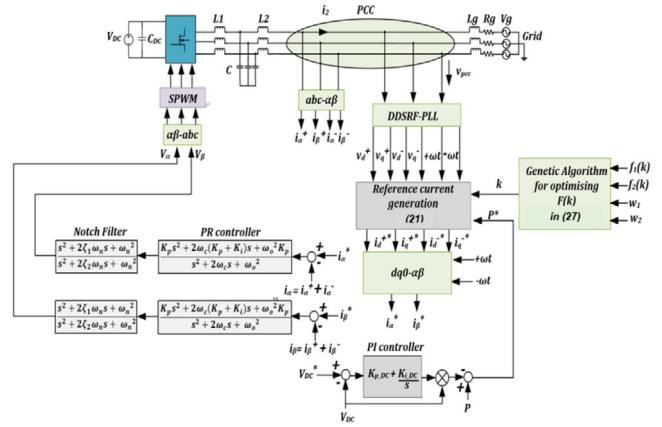


FIGURE 5 Current control layout

phase voltages, the k value evaluated previously is updated and the new reference current for the control loop is estimated.

6 | CONTROL SCHEME

The control scheme must ensure that the VSC delivers accurately the reference current components identified from above according to the required objectives and constraints. A crucial factor for VSC control under unbalanced grid voltage is that it needs to cater for the negative sequence components of both the PCC voltages and converter currents. This requires identifications of both positive and negative phase angles from measured PCC voltages and the decoupled double synchronous reference frame-based phase locking loop (DDSRF-PLL) [7, 26] is applied. Figure 5 shows the proposed control system for the

VSC given in Figure 1 with V_{DC} representing a DC power source voltage which may be from a solar PV generator. The control system consists of four parts: the DDSRF-PLL, the current feedback control loop consisting of the proportional-resonant (PR) controllers and the notch filter, the DC link voltage control and the PWM unit.

As shown in Figure 5, the instantaneous value of the three-phase PCC voltage, v_{pcc} is measured and converted to its equivalent synchronous reference frame using the DDSRF-PLL technique as v_d^+ and v_q^+ , v_d^- and v_q^- . Subsequently, the phase angles for the v_{pcc} positive and negative sequence voltages, $+\omega t$ and $-\omega t$ are determined. These are applied to analyse the instantaneous values of the converter current, i_2 measured at the inverter grid-side terminals. These are converted to the stationary reference frame as i_α^\pm and i_β^\pm using Clarke's transformation and then compared with the stationary reference frame equivalent of the currents $i_d^{\pm*}$ and $i_q^{\pm*}$ for reference current evaluation.

The reference active power, P^* is determined by the DC-bus voltage control loop. With the power source being a solar PV generator, its maximum power value at the sampling instant is applied to compare with the DC power generated by the voltage from the DC-bus feedback control loop times its current. Their error produces the reference power as shown in Figure 5. Following the procedures for the COFPC scheme described in the last sub-section, the reference currents, $i_d^{\pm*}$ and $i_q^{\pm*}$ are then calculated by Equation (21) as illustrated in Figure 4 with the optimal k value determined using the GA. Once the reference current components are determined, they are applied for inverter current control using the PR controller. This employs stationary reference frame, thus the converter reference current, $i_d^{\pm*}$ and $i_q^{\pm*}$ in synchronous reference frame need to be transformed into $i_\alpha^{\pm*}$ and $i_\beta^{\pm*}$. The controller transfer function is expressed as [27]:

$$G_{PR}(s) = K_p + \frac{K_i s}{s^2 + \omega_o^2} \quad (37)$$

where K_p is the proportional gain, K_i is the integral gain and ω_o is the controller resonant frequency which is the fundamental frequency value. For a controller to track a fundamental reference current signal, it must produce an infinitely large gain at the fundamental frequency of the signal. From Equation (37), it is clear that the PR controller would produce an infinite gain if the frequency of the reference signal, ω is equal to the PR controller resonant frequency, ω_o . Thus, Equation (37) becomes:

$$G_{PR}(j\omega_o) = K_p + K_i \frac{s}{-\omega_o^2 + \omega_o^2}. \quad (38)$$

And therefore:

$$G_{PR}(j\omega_o) = \infty. \quad (39)$$

Due to stability problems associated with an infinite gain, a non-ideal PR controller with the following transfer function is

considered [27]:

$$G_{PR}(s) = K_p + K_i \frac{2\omega_c s}{s^2 + 2\omega_c s + \omega_o^2}, \quad (40)$$

where ω_c is the bandwidth around the frequency ω_o .

The input to the PR controller is the current error signal due to the difference between the reference set-point and the measured response signal. As the controller consist of both proportional and integral component, it produces an output signal that is both proportional to the current error signal and proportional to the rate of change of the error signal.

A particular advantage of PR controllers can be noticed when compared to the traditional PI control scheme under unbalanced voltage conditions; since the PR controller provides infinite gain at $\pm \omega_o$, one pair of the controller can simultaneously control both positive and negative sequence current α - β components. However, if we are using PI control scheme, two pairs of controllers, one for positive and the other for negative sequence current components, are required. Thus, the PR controller reduces the number of required controllers by half compared to the PI controller [7]. In addition, it also reduces the computational burden since there is no cross-coupling terms which would exist in PI control scheme since it uses current components in the d-q synchronous reference frame.

Following the PR current controllers, two notch filters (NF) (for α - β) are cascaded in the control loop. These are necessary for actively damping the resonant frequency elements due to the LCL filter connected at the VSC output terminals. The parameters of a NF are tuned to give a complex conjugate pair of zeros capable of cancelling the resonant poles of the LCL filter. The transfer function for the NF is [28]:

$$G_{notch}(s) = \frac{s^2 + 2\zeta_1\omega_n s + \omega_n^2}{s^2 + 2\zeta_2\omega_n s + \omega_n^2}, \quad (41)$$

where ζ_1, ζ_2 are the damping ratios of the zeros and poles respectively, while ω_n is the natural frequency of the notch filter set according to the resonant frequency of the LCL filter.

The outputs of the control loop are the voltage command signals V_α, V_β . These are converted into the stationary abc -frame to provide reference signals to the sine PWM modulator of the VSI.

7 | SIMULATION STUDIES

Simulation studies are performed using a 100 kW solar PV generator as the input power source to validate the proposed COFPC scheme, the results are compared with another two control schemes; BPSC and CAPC. Tables 1 and 2 specify the system and controller parameters respectively.

The performance of the control scheme is investigated for a specified VUF of the PCC voltage, caused by phase A voltage

TABLE 1 System parameters

Parameter	Rating
Inverter rated power (P)	100 kW
$L_1/C/L_2$	3 mH/118 μ F/51 μ H
Grid voltage (V)	380 V (rms)
Grid frequency (f)	50 Hz
DC link voltage (V_{DC})	620 V
Grid impedance (R_g/L_g)	0.1 Ω /0.1 mH
DC link capacitor (C_{DC})	2000 μ F
Notch filter damping ratios (ζ_1/ζ_2)	0.01/1
Switching frequency (f_{sw})	20 kHz

TABLE 2 PI and PR controller parameters

Parameter	Rating
K_p	10
K_i	1500
ω_o	314.2 rad/s
ω_c	0.5 rad/s
K_{p-DC}	0.5
K_{i-DC}	50

dip at time, $t = 0.4$ s. For time, $t < 0.4$ s, PCC voltages are balanced and sinusoidal. The resultant grid currents, active and reactive PV powers, as well as DC link voltages for all control schemes are shown.

It should be noted that the rated current value has to be increased by 20% to accommodate transient surge currents under normal operation without tripping overcurrent devices. With the positive sequence voltage, V^+ at 310 V, the magnitude of I_{rated} according to Equation (34) is 258 A.

7.1 | Optimal k value for 11% VUF

For 11% VUF at the PCC, the optimal value for the decision variable, k from 0 initially, is settled to -0.31 by GA searching. The variation of the corresponding magnitude of the fitness function, $F(k)$ defined by Equation (27), is as shown in Figure 6 which converges finally to about 53% after 57 iterations.

Figure 7a shows the PCC voltage at 11% VUF with the corresponding grid currents in Figure 7b. Phases A and C current variations due to the CAPC scheme have reached the boundary of the rated converter current due to higher negative sequence voltages. However, the current amplitudes from the COFPC are below the rated level, with the BPSC currents remaining equally below the rated value.

Variations of active and reactive powers flowing to the grid due to the three different control schemes are shown in Figure 8a with their corresponding root-mean-square-error (RMSE) values shown in Figure 8b. Setting the reference active power to 100 kW and Q to zero for 11% VUF condition, one

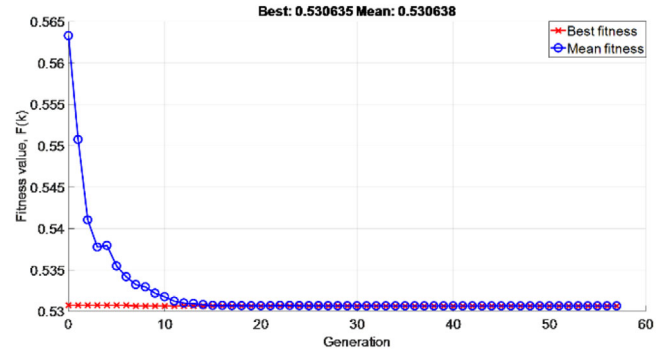


FIGURE 6 Fitness function minimisation for 11% voltage unbalanced factor (VUF) by genetic algorithm (GA) optimisation

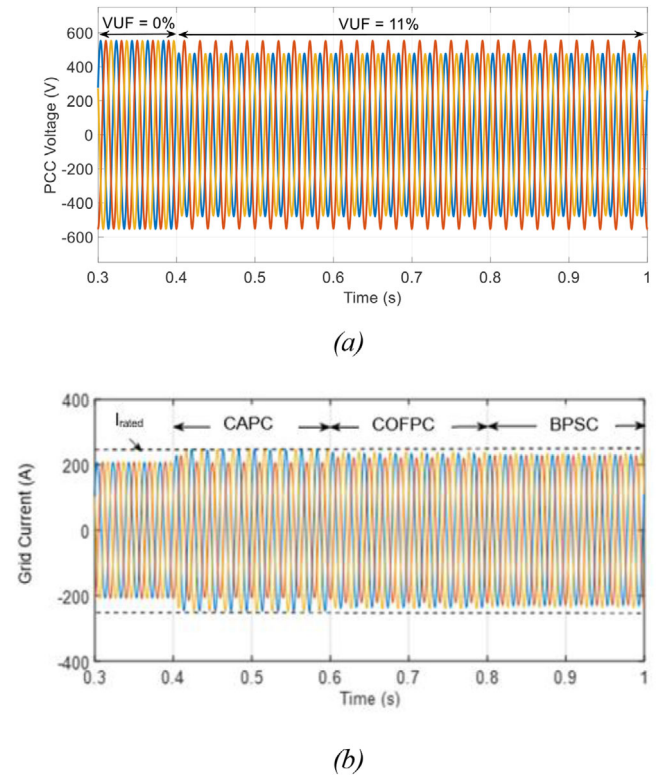


FIGURE 7 11% point of common connection (PCC) voltage unbalance factor (a) point of common connection (PCC) voltage and (b) grid current

can see that there are little active power oscillations from CAPC control. On the other hand, there is active power oscillation by COFPC control but it is about six times lower than that due to BPSC controller.

In terms of reactive power, COFPC gives a better result than that by CAPC as the peak-to-peak oscillation level is 32% lower. With respect to BPSC, Q oscillation is lower than that by COFPC by about 25%.

The DC link voltages and their corresponding RMSE values obtained using the above three control schemes respectively are shown in Figures 9a–b. The BPSC produces the largest ripple voltage with RMSE at about 4.8 V. The COFPC reduces this

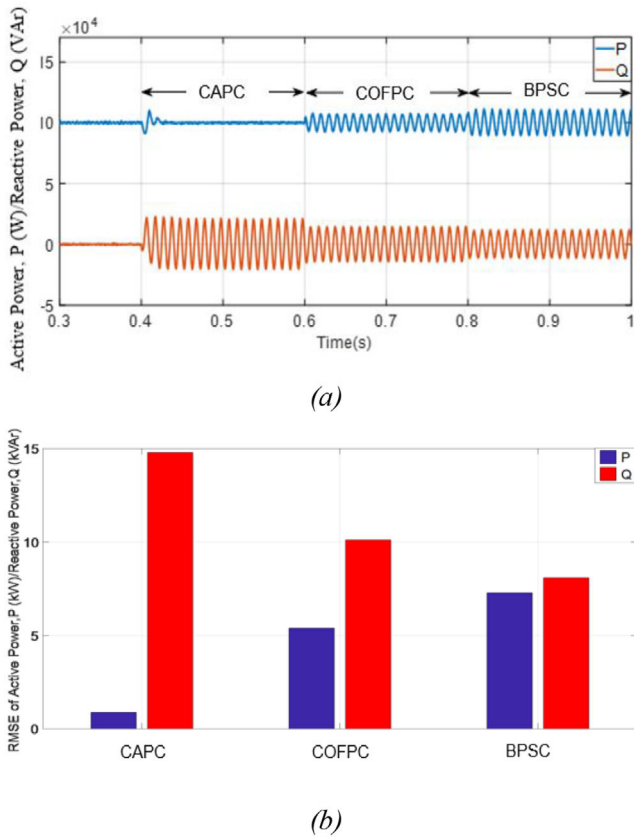


FIGURE 8 11% point of common connection (PCC) voltage unbalance factor (a) active and reactive powers and (b) root-mean-square-error (RMSE) of active and reactive powers

down to 4.4 V. CAPC produces the least ripple with a RMSE of 1.2 V.

From above, the features from COFPC scheme can be seen clearly, it gives a compromised performance in terms of restricting over-current level and suppressing both power oscillations under unbalanced voltage operations. Compared to the CAPC, COFPC has active power oscillation but it offers better performance than CAPC in other aspects since it has much lower reactive power ripple and output current is under the rated limit. Comparing to BPSC, on the other hand, COFPC gives significantly lower active power ripples, though the reactive power ripple is slightly higher. Hence, for VUF at 11%, COFPC offers a solution between the extreme ends of large grid currents and reactive power ripple of the CAPC method and the large active power and DC link fluctuations of the BPSC method.

7.2 | Optimal k value for 18% VUF

Figure 10 shows the optimal value of the decision variable, k obtained from the GA as -0.62 . The mean value of the minimised fitness function has converged to 56% of the amplitude in Equation (27). The number of iterations remain unchanged at 57%.

Figure 11a shows the PCC voltage and the corresponding VUF. At $t > 0.4$ s, the VUF increases to 18%, in response to

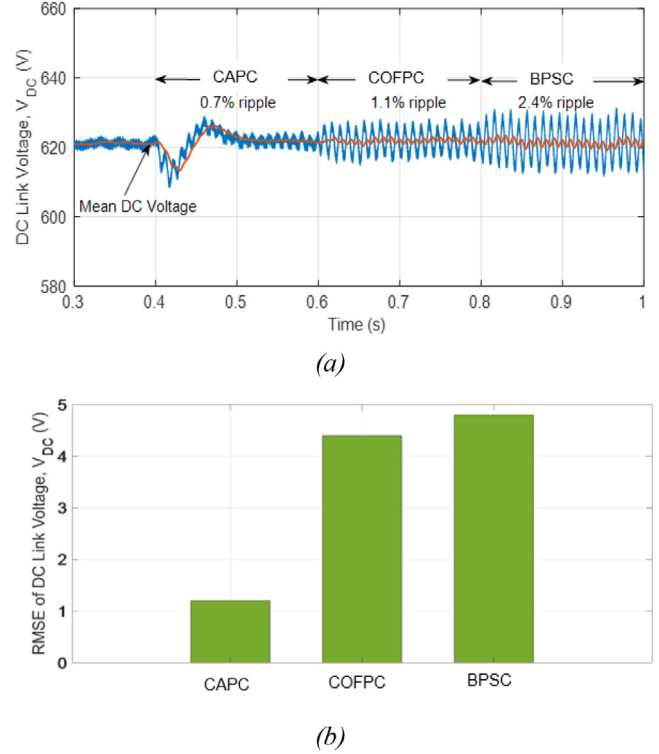


FIGURE 9 11% point of common connection (PCC) voltage unbalance factor (a) DC link voltage and (b) root-mean-square-error (RMSE) of DC link voltage

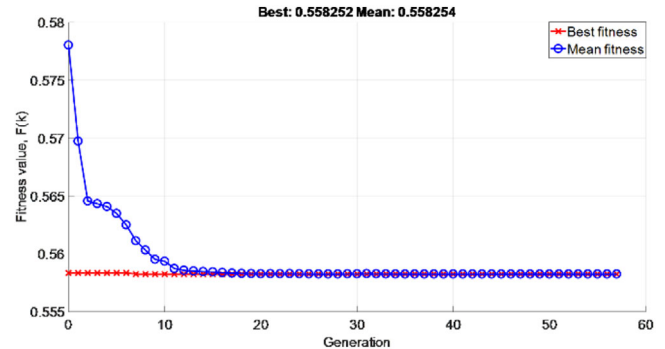


FIGURE 10 Fitness function minimisation for 18% voltage unbalanced factor (VUF) by genetic algorithm (GA) optimisation

a single-phase grid fault. CAPC current amplitudes in phases A and C shown in Figure 11b have exceeded the rating of the inverter currents. With the increase in VUF, the COFPC method has similarly exceeded the rated current with the decision variable determined according to Equation (27). The reference power, P^* has therefore been modified according to Equation (36), with the new reference determined as 90 kW . BPSC current magnitudes have equally increased to the boundary of the rated current with the increased VUF.

Due to a reduced active power set point, the powers in Figures 12a–b show the COFPC active and reactive power ripples decrease, as both are functions of the active power reference, as described by Equations (22) and (23) respectively. The

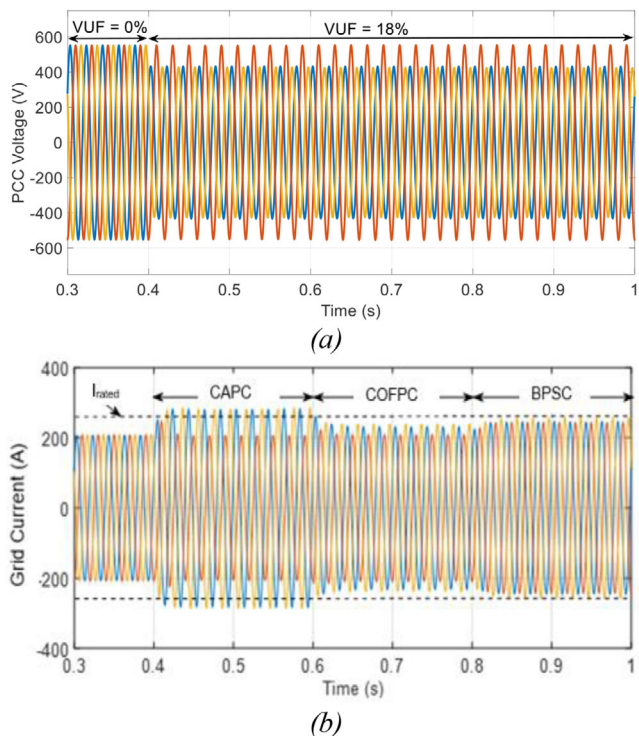


FIGURE 11 18% point of common connection (PCC) voltage unbalance factor (a) point of common connection (PCC) voltage and (b) grid current

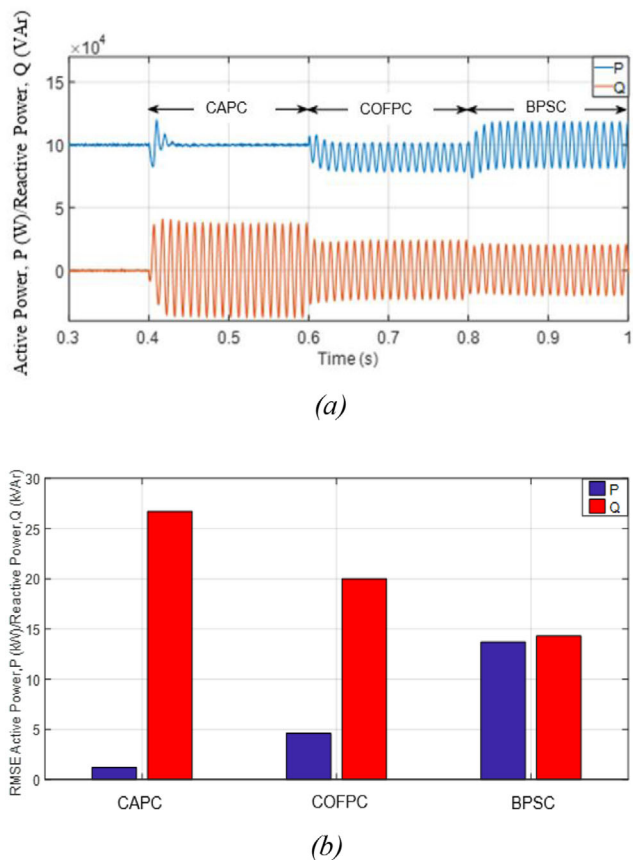


FIGURE 12 18% point of common connection (PCC) voltage unbalance factor (a) active and reactive powers and (b) root-mean-square-error (RMSE) of active and reactive powers

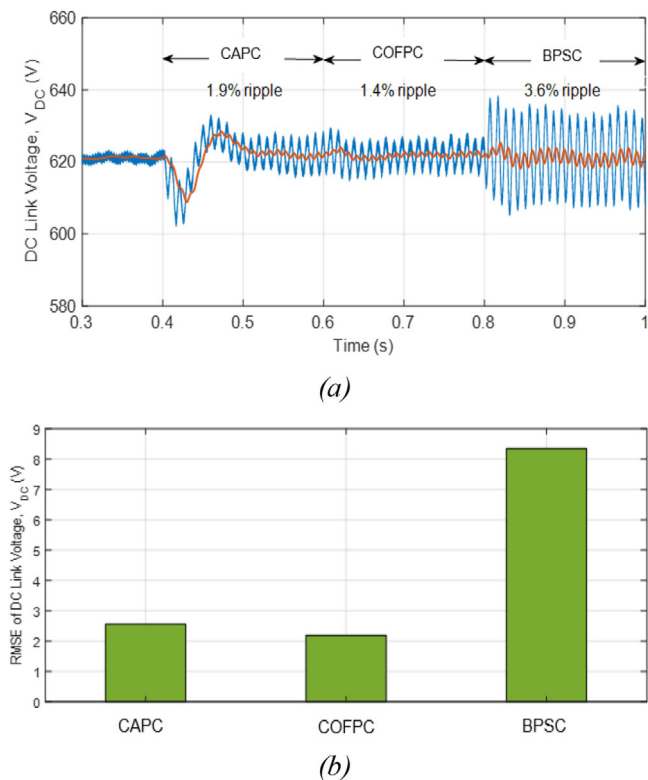


FIGURE 13 18% point of common connection (PCC) voltage unbalance factor (a) DC link voltage and (b) root-mean-square-error (RMSE) of DC link voltage

COFPC has decreased the active power ripple by 66% compared to the BPSC. However, its active power fluctuations are approximately 4 times larger than that produced by the CAPC. In terms of reactive power, the COFPC has reduced the ripples by 25% when compared with the CAPC method. With the BPSC method as reference point, the COFPC has increased the reactive power oscillations by 28%.

The DC link voltage and its corresponding RMSE values are shown in Figures 13a–b. Due to the reduction in power set-point, the COFPC has the least DC link voltage ripple, reducing the fluctuation by 14% compared to the CAPC method and 74% compared to the BPSC method. Although the active power delivered by the COFPC has been curtailed due to the maximum current constraint when the VUF is 18%, the active power and DC link voltage fluctuations have been significantly minimised. This can be considered a huge advantage, as the reduced ripple at the DC link makes it possible to use lower capacitor values, which is more economical.

8 | CONCLUSION

The paper has presented a novel optimisation method of reducing active and reactive power ripples in a grid connected converter in the presence of grid voltage unbalance. The power ripples are formulated as a MOOP and the decision variable, ℓ is chosen based on the GA. Simulation results have compared

the operations of the proposed COFPC with two other classical methods: the CAPC and the BPSC. The BPSC has the advantage of injecting a balanced set of currents to the grid at the expense of large active power and DC link fluctuations. The proposed COFPC provides a compromised solution between the extreme ends of large converter currents and reactive power ripple of the CAPC method and the large active power and DC link fluctuations of the BPSC method. Additionally, the GA in the COFPC imposes a maximum limit on the reference currents, ensuring that regardless of VUF, the inverter current rating is never exceeded. Through the constraints of both DC link voltage ripple and maximum inverter current, the COFPC provides an advantage compared to other conventional methods of control under unbalanced grid voltage conditions.

ACKNOWLEDGEMENTS

N. Rufa'I would like to thank the Tertiary Education Trust Fund (TETFUND), Nigeria and the British Federation for Women Graduates (BFWG) and UK for their sponsorship.

ORCID

Nabila Ahmed Rufa'I  <https://orcid.org/0000-0002-5340-1479>

REFERENCES

- Li, J.: Measurement and Analysis of Overvoltages in Power Systems. Wiley, New York (2018)
- Blackburn, J.L., Domin, T.J.: Protective Relaying: Principles and Applications. CRC Press, Boca Raton, FL (2015)
- Al-Shetwi, A.Q., et al.: Power quality assessment of grid-connected PV system in compliance with the recent integration requirements. *Electronics* 9(2), 366 (2020)
- Jia, J. et al.: A review on grid-connected converter control for short-circuit power provision under grid unbalanced faults. *IEEE Trans. Power Delivery* 33(2), 649–661 (2018)
- Çelik, D., Meral, M.E.: Voltage support control strategy of grid-connected inverter system under unbalanced grid faults to meet fault ride through requirements. *IET Gener. Transm. Distrib.* 14(16), 3198–3210 (2020)
- Naderipour, A., et al.: Optimal designing of static var compensator to improve voltage profile of power system using fuzzy logic control. *Energy* 192, 116665 (2020)
- Teodorescu, R., Liserre, M., Rodriguez, P.: Grid Converters for Photovoltaic and Wind Power Systems. John Wiley & Sons, New York (2011)
- Cupertino, A.F., et al.: Benchmarking of power control strategies for photovoltaic systems under unbalanced conditions. *Int. J. Electr. Power Energy Syst.* 106, 335–345 (2019)
- Wang, Y., et al.: Power-current coordinated control without sequence extraction under unbalanced voltage conditions. *IET Power Electron.* 13(11), 2274–2280, (2020)
- Lo, Y.-H., et al.: An iterative control method for voltage source converters to eliminate uncharacteristic harmonics under unbalanced grid voltages for high-power applications. *IEEE Trans. Sustainable Energy* 10(3), 1419–1429 (2018)
- Somkun, S.: Unbalanced synchronous reference frame control of single-phase stand-alone inverter. *Int. J. Electr. Power Energy Syst.* 107, 332–343 (2019)
- Akagi, H., et al.: Instantaneous Power Theory and Applications to Power Conditioning. John Wiley & Sons, New York (2017)
- Wang, F., Duarte, J.L., Hendrix, M.A.: Active power control strategies for inverter-based distributed power generation adapted to grid-fault ride-through requirements. In: 13th European Conference on Power Electronics and Applications, EPE'09., Barcelona, Spain, 8-10 September 2009
- Cai, X., et al.: A grid weighted sum Pareto local search for combinatorial multi and many-objective optimization. *IEEE Trans. Cybern.* 49(9), 3586–3598 (2018)
- Pang, L.M., et al: Decomposition-based multi-objective evolutionary algorithm design under two algorithm frameworks. *Neural Evol. Comput.* 8, 163197–163208 (2020)
- Konak, A., Coit, D.W., Smith, A.E.: Multi-objective optimization using genetic algorithms: A tutorial. *Reliab. Eng. Syst. Saf.* 91(9), 992–1007 (2006)
- Kamal, M., et al.: A distance based method for solving multi-objective optimization problems. *J. Mod. Appl. Stat. Methods* 17(1), 21 (2018)
- Wang, Y., et al.: Multi-objective optimization of rolling schedule for tandem cold strip rolling based on NSGA-II. *J. Manuf. Processes* 60, 257–267 (2020)
- Marler, R.T., Arora, J.S.: The weighted sum method for multi-objective optimization: New insights. *Struct. Multidiscip. Optim.* 41(6), 853–862 (2010)
- Wang, F., Duarte, J., Hendrix, M.: Design and analysis of active power control strategies for distributed generation inverters under unbalanced grid faults. *IET Gener. Transm. Distrib.* 4(8), 905–916 (2010)
- Abad, G., Power Electronics and Electric Drives for Traction Applications. John Wiley & Sons, New York (2016)
- Chambers, L.D., Practical Handbook of Genetic Algorithms: Complex Coding Systems. CRC Press, Boca Raton, FL (2019)
- Momoh, J.A., Electric Power System Applications of Optimization. CRC Press, Boca Raton, FL (2017)
- Bhargava, S.: A note on evolutionary algorithms and its applications. *Adult Learn. Math Int. J.* 8(1), 31–45 (2013)
- As karzadeh, A.: A memory-based genetic algorithm for optimization of power generation in a microgrid. *IEEE Trans. Sustainable Energy* 9(3), 1081–1089 (2017)
- Miletic, Z., et al.: Optimal control of three-phase PV inverter under grid voltage unbalance. In 21st European Conference on Power Electronics and Applications (EPE'19 ECCE Europe), Geneva, Italy, 3-5 September 2019
- Hung, V.T., et al.: Double-loop control structure using proportional resonant and sequence-decoupled resonant controllers in static coordinates for dynamic voltage restorer. *Chin. J. Electr. Eng.* 5(3), 10–19 (2019)
- Rufa'I, N.A., Zhang, L., Chong, B.: Performance analysis of adaptive notch filter active damping methods for grid-connected converters under a varying grid impedance. In 12th IEEE PES Power Tech Conference IEEE, Manchester, UK, 18-22 June 2017

How to cite this article: Rufa'I NA, Zhang L, Chong B. Constrained optimised flexible power control for grid-connected converters under unbalanced faults. *J. Eng.* 2021;2021:321–333. <https://doi.org/10.1049/tje2.12038>

APPENDIX

DERIVATION OF MAXIMUM CONVERTER CURRENT

The phase current through the converter (phase A) can be expressed in the stationary reference frame as:

$$I_a = \sqrt{I^{+2} + I^{-2} + 2I^+I^- \cos \alpha}, \quad (\text{A.1})$$

where I^+ and I^- are the magnitudes of the positive and the negative sequence current components expressed as:

$$I^+ = \sqrt{I_d^{+2} + I_q^{+2}} \tag{A.2}$$

and

$$I^- = \sqrt{I_d^{-2} + I_q^{-2}}. \tag{A.3}$$

Substituting for currents from Equation (21) into (A.1) leads to:

$$I_a = \frac{P\sqrt{A + k^2B + 2k\sqrt{AB} \cos \alpha}}{1.5 [A + kB]}, \tag{A.4}$$

where

$$A = \|v_d^+\|^2 + \|v_q^+\|^2, \tag{A.5}$$

$$B = \|v_d^-\|^2 + \|v_q^-\|^2, \tag{A.6}$$

$$\alpha = \theta^+ + \theta^- - \varphi \tag{A.7}$$

and θ^+, θ^- are the phase angles of the positive and the negative sequence PCC voltages respectively, while

$$\varphi = \tan^{-1} \frac{v_q^+}{v_d^+} + \tan^{-1} \frac{v_q^-}{v_d^-}. \tag{A.8}$$

The peak value occurs when $\theta^+ + \theta^- = \varphi$. Hence, (A.4) becomes:

$$I_{a(\max)} = \frac{P\sqrt{A + k^2B + 2k\sqrt{AB}}}{1.5 [A + kB]}. \tag{A.9}$$

The peak values for phases B and C are equal in magnitude to (A.9) but occur at phase angles $\alpha - \frac{2}{3}\pi$ and $\alpha + \frac{2}{3}\pi$ respectively.